

Adaptive Target Detection for FDA-MIMO Radar with Training Data in Gaussian noise

Ping Li, Bang Huang, *Graduate Student Member, IEEE*, Wen-Qin Wang* *Senior Member, IEEE*

Abstract—This paper addresses the problem of detecting a moving target embedded in Gaussian noise with an unknown covariance matrix for frequency diverse array multiple-input multiple-output (FDA-MIMO) radar. To end it, assume that obtaining a set of training data is available. Moreover, we propose three adaptive detectors in accordance with the one-step generalized likelihood ratio test (GLRT), two-step GLRT, and Rao criteria, namely OGLRT, TGLRT, and Rao. The LH adaptive matched filter (LHAMF) detector is also introduced when decomposing the Rao test. Next, all provided detectors have constant false alarm rate (CFAR) properties against the covariance matrix. Besides, the closed-form expressions for false alarm probability (PFA) and detection probability (PD) are derived. Finally, this paper substantiates the correctness of the aforementioned algorithms through numerical simulations.

Index Terms—Frequency diverse array multiple-input multiple-output (FDA-MIMO), detection, GLRT, Rao, AMF, mismatch.

I. INTRODUCTION

FREQUENCY diverse array (FDA) radar, as introduced by Antonik et al. [1], employs diverse transmitting carrier frequencies across adjacent elements, resulting in a range-angle-time-dependent beampattern [2]–[4] and even a time-varying radar cross-section (RCS) [5]. While some radar scholars have focused on designing the transmit beampattern [6]–[8], various applications for FDA radar have emerged, such as low probability of intercept (LPI) [9], lamb wave sensing [3], and others [10], [11]. However, the time-varying and range-angle coupling beampattern of FDA radar make it difficult to utilize for effective target detection and localization [12]–[14]. In response to this, scholars have proposed combining multiple-input multiple-output (MIMO) radar [15], [16] with FDA radar technology to form FDA-MIMO radar [17]–[19]. It is worth noting that FDA-MIMO radar proves effective in eliminating time-varying effects and decoupling range and angle dependencies in the beampattern [19]–[21]. Therefore, this paper primarily delves into the adaptive target detection technology enabled by FDA-MIMO radar.

Moreover, [4] analyzed the generalized ambiguity function (GAF) of FDA and concluded that FDA-MIMO had been endowed with the abilities, namely super range resolution

and resolving the Doppler ambiguity. Further, the nature of super-resolution in the range domain has further validated the effectiveness of what FDA-MIMO radar can suppress the main-lobe deceptive jamming/clutter [13], [21], [22]. The reason is that FDA-MIMO can distinguish the echoes from different ranges [13]. On the other side, Wan [23] utilized the characteristic of multiple frequencies of FDA-MIMO radar to resolve the Doppler ambiguity for high-speed moving target. Meanwhile, there also arise applications in other fields, such as high-resolution and wide-swath synthetic aperture radar (SAR) imaging [24], SAR ground moving target indication (GMTI) [25], deceptive jamming against SAR [26] and etc [27]–[29].

The range-dependent property of FDA-MIMO radar makes obtaining homogenous training data in clutter challenging. Therefore, some studies have designed target detectors for FDA-MIMO radar without needing training data [12], [30]. Specifically, Huang *et al.* [12] presented the detectors resorting to Rao and Wald criteria, respectively. Furthermore, leveraging the super-resolution characteristics of FDA radar in range dimension [31], the same authors investigated the problem of distributed targets spanning one primary range cell and multiple sub-range cells [32]. Nevertheless, determining the detection threshold for the detectors above can be challenging in practical scenarios. One approach is to derive the detection threshold from an extensive historical data set. However, when historical data fails to represent the current environment adequately, these detectors may not function optimally.

Considering an FDA-MIMO radar system operating in a noise environment, including receiver thermal noise, jammers, and clutter after secondary range compensation [33]–[35], homogeneous training data can be obtained from adjacent cells to estimate the unknown covariance matrix. Hence, to detect the target embedded in Gaussian interference, Lan *et al.* employed semidefinite programming (SDP) to determine the optimal frequency offset for detection, and developed a one-step GLRT (OGLRT) detector [13]. Further, based on the two-step GLRT (TGLRT) and model order selection (MOS) criteria, [36] presented a detector that can simultaneously achieve target detection and recognition. Zeng *et al.* [37] investigated the moving target detection problem by considering the situations with known and unknown Doppler shifts, respectively, according to the OGLRT criterion. It is worth noting that there is an error in the analysis of the statistical characteristics of the detectors in [37], and this error will be rectified in this paper. Meanwhile, to the best of author's knowledge, there were no relevant studies based on TGLRT and Rao criteria to study the detection problem provided in [37]. Nevertheless, previous excellent published works [38]–

This work was supported by National Natural Science Foundation of China 62171092. (Corresponding author: Wen-Qin Wang)

Ping, Li, Bang, Huang and Wen-Qin, Wang are with School of Information and Communication Engineering, University of Electronic Science and Technology of China, Chengdu, 611731, P. R. China. Wen-Qin Wang is also with the Yangtze Delta Region Institute (Huzhou), University of Electronic Science and Technology of China, Huzhou, 313001, P. R. China. (Emails:202122220102@std.uestc.edu.cn; huang-bang@std.uestc.edu.cn; wqwang@uestc.edu.cn)

[42] indicated that, in comparison to the OGLRT, both the TGLRT and Rao detectors exhibit superior detection performance, with a notable emphasis on robustness and selectivity for mismatched signals. These observations have motivated us to conduct a more in-depth investigation into this issue.

Moreover, the detection problem investigated in this paper is a specific form of the detection model introduced in [43], [44]. Differently, this study's unique application of the model to the FDA-MIMO radar system distinguishes it. Furthermore, this paper goes beyond merely analysing the proposed detectors' statistical properties, presenting closed-form expressions for the probability of false alarm (PFA) and probability of detection (PD). Additionally, this study delves into the implications of Doppler dimension mismatch through thorough numerical simulation.

This paper addresses the challenge of detecting a moving target embedded in Gaussian noise with an unknown covariance matrix for FDA-MIMO radar. The main contributions are summarized as follows:

- When training data is available, we design three adaptive detectors to detect a moving target embedded in an unknown Gaussian noise (includes thermal noise, jammers, and clutter after secondary range compensation)—specifically, OGLRT, TGLRT, and Rao. Additionally, an LHAMF detector is proposed when decomposing the Rao detector.
- A comprehensive statistical analysis is conducted for the proposed detectors, providing closed-form expressions for the PFA and PD for four detectors. We also demonstrate their constant false alarm rate (CFAR) properties against covariance matrix under null hypothesis.
- Simulation results highlight the validity of proposed methods. OGLRT and LHAMF excel in scenarios with no signal mismatch, while TGLRT demonstrates robustness, and the Rao detector exhibits optimal selectivity for mismatched signal situations. Moreover, FDA-MIMO consistently outperforms traditional MIMO in detecting target operating in the presence of Gaussian noise plus mainlobe deceptive jamming.

The subsequent structure of the paper is organized as follows. In Section II, we formulate the problem of detecting a moving target as a binary hypothesis. Following that, in Section III, three detectors are designed. Section IV provides a detailed analysis of the statistical characteristics of the proposed detectors. Section V gives the simulation results, and finally, the conclusion is provided in Section VI.

Notations: Matrices (vectors) are defined by boldface letters. $\mathbb{C}^{M \times N}$ is a complex matrix with dimension of $M \times N$. The symbol $(\cdot)^\dagger$, $(\cdot)^T$ and $(\cdot)^*$ denote conjugate transpose, transpose and complex conjugate, respectively. \sim means “be distributed as”, and \mathcal{CF} denotes F-distribution. \mathcal{CN} , \mathcal{CW} and \mathcal{CB} represents the Gaussian, Wishart and Beta distribution, respectively. Hadamard product and Kronecker product are denoted by \odot and \otimes , respectively. $\text{Tr}[\cdot]$ and $\det[\cdot]$ represent the trace and determinant of the matrix, respectively. $\ln(\cdot)$ and $\partial(\cdot)$ denote the logarithm function and gradient operator, respectively. $\text{vec}[\cdot]$ represents the vectorization operation, and $E(\cdot)$ is the statistical expectation. \mathbf{I} and cont. denote an

identity matrix with appropriate dimension and a constant. $\mathbf{P}_B = \mathbf{B}(\mathbf{B}^\dagger \mathbf{B})^{-1} \mathbf{B}^\dagger$ is an orthogonal projection matrix onto the subspace spanned by the columns of \mathbf{B} , and $\mathbf{P}_B^\perp = \mathbf{I} - \mathbf{P}_B$. $\text{Re}[\cdot]$ and $\text{Im}[\cdot]$ represent the real and imaginary parts of a complex number, respectively. $[\mathbf{B}]_k$ denotes the k th column of matrix \mathbf{B} .

II. PROBLEM FORMULATION

Assuming that there are M FDA transmit and N phased-array (PA) receive elements in a colocated FDA-MIMO radar system. Regarding the first element as the reference element, the carrier frequency of m th element can be denoted by

$$f_m = f_0 + \Delta f_m, m = 1, 2, \dots, M, \quad (1)$$

where f_0 is the carrier frequency of first element and $\Delta f_m = (m - 1)\Delta f$ is the frequency offset between the first and m th element. Under the far-field assumption, consider a point-like target with a radial velocity v , located at the distance of r and the angle of θ . Then, the received signal [12], [45], [46] at k th ($k = 1, \dots, K$) snapshot can be expressed as

$$\mathbf{z}_k = \xi \omega_k(f_d) \mathbf{a}_{\text{TR}}(r, \theta) + \mathbf{n}_k \in \mathbb{C}^{MN}, \quad (2)$$

where ξ encompass both the target and channel effects, is unknown. $\omega_k(f_d) = e^{j2\pi f_d t}$ is the Doppler shift caused by the moving target, with $f_d = \frac{2v}{c} f_0 T_p$. c and T_p represent the light speed and pulse repetition interval (PRI), respectively. Moreover, $\mathbf{a}_{\text{TR}}(r, \theta)$ denotes the joint transmitting-receiving steering vector, defined as

$$\mathbf{a}_{\text{TR}}(r, \theta) = \mathbf{a}_T(r, \theta) \otimes \mathbf{a}_R(\theta) \in \mathbb{C}^{MN}, \quad (3)$$

where $\mathbf{a}_R(\theta)$ represents receiving steering vector, given by

$$\mathbf{a}_R(\theta) = \left[1, e^{j2\pi \frac{d_R \sin \theta}{\lambda_0}}, \dots, e^{j2\pi(M-1) \frac{d_R \sin \theta}{\lambda_0}} \right] \in \mathbb{C}^N, \quad (4)$$

and $\mathbf{a}_T(r, \theta)$ is the transmitting steering vector, with

$$\mathbf{a}_T(r, \theta) = \mathbf{a}_t(\theta) \odot \mathbf{e}(-r), \quad (5)$$

where

$$\begin{aligned} \mathbf{a}_t(\theta) &= \left[1, e^{j2\pi \frac{d_T \sin \theta}{\lambda_0}}, \dots, e^{j2\pi(M-1) \frac{d_T \sin \theta}{\lambda_0}} \right] \in \mathbb{C}^M, \\ \mathbf{e}(r) &= \left[1, e^{j2\pi \Delta f \frac{2r}{c}}, \dots, e^{j2\pi(M-1) \Delta f \frac{2r}{c}} \right] \in \mathbb{C}^M. \end{aligned} \quad (6)$$

The symbol $\frac{2r}{c}$ is the time delay for the signal to travel from the first transmitting element to the target and back to the first receiving element. d_T and d_R are the distance between transmit and receive element, respectively.

Hence, with K snapshots, the received signal can be expressed as

$$\mathbf{Z} = \xi \mathbf{a}_{\text{TR}}(r, \theta) \boldsymbol{\omega}_D^T(f_d) + \mathbf{N} \in \mathbb{C}^{MN \times K}, \quad (7)$$

where

$$\begin{aligned} \mathbf{Z} &= [\mathbf{z}_0, \mathbf{z}_1, \dots, \mathbf{z}_{K-1}] \in \mathbb{C}^{MN \times K} \\ \mathbf{N} &= [\mathbf{n}_0, \mathbf{n}_1, \dots, \mathbf{n}_{K-1}] \in \mathbb{C}^{MN \times K} \\ \boldsymbol{\omega}_D(f_d) &= [\omega_0(f_d), \omega_1(f_d), \dots, \omega_{K-1}(f_d)] \in \mathbb{C}^K. \end{aligned} \quad (8)$$

Let \mathcal{H}_1 hypothesis and \mathcal{H}_0 hypothesis represent the presence and absence of a point-like target in the test data, respectively. Therefore, the detection problem interested can be modeled as a binary hypothesis, given by

$$\begin{cases} \mathcal{H}_1 : \begin{cases} \mathbf{Z} = \xi \mathbf{a}_{\text{TR}}(r, \theta) \boldsymbol{\omega}_{\text{D}}^T(f_d) + \mathbf{N} \\ \mathbf{Z}_l = \mathbf{N}_l, l = 1, 2, \dots, L \end{cases} \\ \mathcal{H}_0 : \begin{cases} \mathbf{Z} = \mathbf{N} \\ \mathbf{Z}_l = \mathbf{N}_l, l = 1, 2, \dots, L \end{cases} \end{cases} \quad (9)$$

where $\mathbf{Z}_l = \mathbf{N}_l \in \mathbb{C}^{MN \times K}, l = 1, 2, \dots, L$ is the homogenous training data obtained from adjacent cells with L being number of neighbouring bins. Each column of \mathbf{N} and $\mathbf{N}_l, l = 1, 2, \dots, L$ is an independent and identically distributed (IID) zero-mean complex-valued Gaussian random vector with an unknown covariance matrix \mathbf{R} .

Compared with the published works [12], [46], this paper will study the detection problem (9) with the aid of training data term $\mathbf{Z}_l, l = 1, 2, \dots, L$. Moreover, different from [37], this study designs additional adaptive detectors based on the TGLRT and Rao criteria. Furthermore, we will correct statistical analysis errors in [37] for OGLRT detector. Finally, it is worth noting that the detection problem (9) aligns with a specific instantiation of the detection model outlined in [43], [44]. However, what sets this study apart is its distinctive application of the model to the FDA-MIMO radar system. Moreover, beyond a mere analysis of the statistical properties of the proposed detectors, this paper provides closed-form expressions for the PFA and PD.

III. DETECTORS DESIGN

In this section, detectors will be designed based on OGLRT, TGLRT and Rao criteria, to determine the presence or absence of the moving target from received data.

Define

$$\mathbf{Y} = [\mathbf{Z}_1, \mathbf{Z}_2, \dots, \mathbf{Z}_L] \in \mathbb{C}^{MN \times KL}, \quad (10)$$

and $\mathbf{S} = \mathbf{Y}\mathbf{Y}^\dagger$ is the sample covariance matrix (SCM). Notably, to ensure \mathbf{S} is invertible, we need $LK > MN$.

The joint probability density function (PDF) of \mathbf{Z} and \mathbf{Y} under \mathcal{H}_1 can be expressed as

$$\begin{aligned} f(\mathbf{Z}, \mathbf{Y} | \xi, \mathbf{R}, \mathcal{H}_1) &= \frac{1}{\pi^{MNK(L+1)} \det^{K(L+1)}(\mathbf{R})} \\ &\times \exp \left\{ -\text{Tr} \left[\mathbf{R}^{-1} \mathbf{Z}_1 \mathbf{Z}_1^\dagger \right] - \text{Tr} \left[\mathbf{R}^{-1} \mathbf{S} \right] \right\} \end{aligned} \quad (11)$$

where

$$\mathbf{Z}_1 = \mathbf{Z} - \xi \mathbf{a}_{\text{TR}}(r, \theta) \boldsymbol{\omega}_{\text{D}}^T(f_d). \quad (12)$$

Similarly, the joint PDF under \mathcal{H}_0 is

$$\begin{aligned} f(\mathbf{Z}, \mathbf{Y} | \mathbf{R}, \mathcal{H}_0) &= \frac{1}{\pi^{MNK(L+1)} \det^{K(L+1)}(\mathbf{R})} \\ &\times \exp \left\{ -\text{Tr} \left[\mathbf{R}^{-1} \mathbf{Z}\mathbf{Z}^\dagger \right] - \text{Tr} \left[\mathbf{R}^{-1} \mathbf{S} \right] \right\}. \end{aligned} \quad (13)$$

A. OGLRT

As shown in Appendix A, the OGLRT detector can be given by

$$\Lambda = \frac{\tilde{\mathbf{a}}^\dagger \left(\mathbf{I} + \tilde{\mathbf{Z}} \mathbf{P}_{\tilde{\omega}_{\text{D}}^*(f_d)}^\perp \tilde{\mathbf{Z}}^\dagger \right)^{-1} \tilde{\mathbf{a}}}{\tilde{\mathbf{a}}^\dagger \left(\mathbf{I} + \tilde{\mathbf{Z}} \tilde{\mathbf{Z}}^\dagger \right)^{-1} \tilde{\mathbf{a}}} \underset{\mathcal{H}_0}{\overset{\mathcal{H}_1}{\gtrless}} \lambda. \quad (14)$$

with

$$\tilde{\mathbf{Z}} = \mathbf{S}^{-1/2} \mathbf{Z}, \quad (15)$$

$$\tilde{\mathbf{a}} = \mathbf{S}^{-1/2} \mathbf{a}_{\text{TR}}(r, \theta). \quad (16)$$

It is essential to highlight that (14) is identical to the detector Eq.(24) in [37]. However, the authors believe there are some errors in the statistical analysis conducted by [37]. These concerns will be further verified by the theoretical derivation and numerical simulations in Section IV-A and Section V. Additionally, regarding structure, OGLRT resembles Kelly's GLRT (KGLRT) [47], and the distinctions between them will also be detailed in Section IV-A.

B. TGLRT

Suppose the covariance matrix \mathbf{R} is known in advance, the decision statistic of TGLRT criterion [41] can be written as

$$\Lambda_{TGLRT} = \frac{\max_{\xi} f(\mathbf{Z}, \mathbf{Y} | \xi, \mathbf{R}, \mathcal{H}_1)}{\max_{\xi} f(\mathbf{Z}, \mathbf{Y} | \mathbf{R}, \mathcal{H}_0)} \underset{\mathcal{H}_0}{\overset{\mathcal{H}_1}{\gtrless}} \lambda. \quad (17)$$

Inserting (11) and (13) into (17) results in

$$\Lambda_{TGLRT} = \max_{\xi} e^{\left\{ \text{Tr}[\mathbf{R}^{-1} \mathbf{Z}\mathbf{Z}^\dagger] - \text{Tr}[\mathbf{R}^{-1} \mathbf{Z}_1 \mathbf{Z}_1^\dagger] \right\}} \underset{\mathcal{H}_0}{\overset{\mathcal{H}_1}{\gtrless}} \lambda. \quad (18)$$

Then, define

$$g(\xi) = \text{Tr} \left[\mathbf{R}^{-1} \mathbf{Z}_1 \mathbf{Z}_1^\dagger \right], \quad (19)$$

Derivative $g(\xi)$ with respect to (w.r.t.) ξ , yields

$$\frac{\partial g(\xi)}{\partial \xi} = \boldsymbol{\omega}_{\text{D}}^T(f_d) \left(\mathbf{Z} - \xi \mathbf{a}_{\text{TR}}(r, \theta) \boldsymbol{\omega}_{\text{D}}^T(f_d) \right)^\dagger \mathbf{R}^{-1} \mathbf{a}_{\text{TR}}(r, \theta). \quad (20)$$

Equating $\frac{\partial g(\xi)}{\partial \xi}$ to zero gives the maximum likelihood estimation (MLE) of ξ , as

$$\hat{\xi} = \frac{\mathbf{a}_{\text{TR}}^\dagger(r, \theta) \mathbf{R}^{-1} \mathbf{Z} \boldsymbol{\omega}_{\text{D}}^*(f_d)}{\mathbf{a}_{\text{TR}}^\dagger(r, \theta) \mathbf{R}^{-1} \mathbf{a}_{\text{TR}}(r, \theta) \boldsymbol{\omega}_{\text{D}}^T(f_d) \boldsymbol{\omega}_{\text{D}}^*(f_d)}. \quad (21)$$

Plugging (21) into (19), leads to

$$g(\hat{\xi}) = \text{Tr} \left[\mathbf{Z}^\dagger \mathbf{R}^{-1} \mathbf{Z} - \hat{\xi} \boldsymbol{\omega}_{\text{D}}^T(f_d) \mathbf{Z}^\dagger \mathbf{R}^{-1} \mathbf{a}_{\text{TR}}(r, \theta) \right]. \quad (22)$$

Substituting (22) into (18) and taking the logarithm of the result yield the expression for the TGLRT detector for known \mathbf{R} , given by

$$\Lambda_{TGLRT} = \frac{\mathbf{a}_{\text{TR}}^\dagger(r, \theta) \mathbf{R}^{-1} \mathbf{Z} \boldsymbol{\omega}_{\text{D}}^*(f_d) \boldsymbol{\omega}_{\text{D}}^T(f_d) \mathbf{Z}^\dagger \mathbf{R}^{-1} \mathbf{a}_{\text{TR}}(r, \theta)}{\mathbf{a}_{\text{TR}}^\dagger(r, \theta) \mathbf{R}^{-1} \mathbf{a}_{\text{TR}}(r, \theta) \boldsymbol{\omega}_{\text{D}}^T(f_d) \boldsymbol{\omega}_{\text{D}}^*(f_d)} \underset{\mathcal{H}_0}{\overset{\mathcal{H}_1}{\gtrless}} \lambda. \quad (23)$$

However, in practice, \mathbf{R} is so unknown that (23) cannot be directly used. As a consequence, replacing \mathbf{R} in (23) with

SCM \mathbf{S} , the final TGLRT detector for the problem interested can be given by

$$\Lambda_{TGLRT} = \frac{|\tilde{\mathbf{a}}^\dagger \tilde{\mathbf{Z}}_\omega|^2}{\tilde{\mathbf{a}}^\dagger \tilde{\mathbf{a}}} \underset{\mathcal{H}_0}{\overset{\mathcal{H}_1}{\geq}} \lambda, \quad (24)$$

where

$$\tilde{\mathbf{Z}}_\omega = \tilde{\mathbf{Z}} \frac{\boldsymbol{\omega}_D^*(f_d)}{\sqrt{\boldsymbol{\omega}_D^T(f_d) \boldsymbol{\omega}_D^*(f_d)}}. \quad (25)$$

If we consider $\tilde{\mathbf{Z}}_\omega$ as the received data, (24) shares the same form as the detector proposed by Robey *et al.* [41]. However, the critical distinction is that the received data in (25) also includes the Doppler information of the moving target. Given the established equivalence between TGLRT and the Wald test [40], we avoid designing detectors based on the Wald criterion in this paper.

C. Rao

Assuming that $\boldsymbol{\Theta}$ is a parameter vector, defined as

$$\boldsymbol{\Theta} = [\boldsymbol{\Theta}_r^T, \boldsymbol{\Theta}_s^T]^T, \quad (26)$$

where, $\boldsymbol{\Theta}_r = [\xi_R, \xi_I]$ is useful parameter vector, with ξ_R and ξ_I represent real and imaginary parts of ξ , respectively. $\boldsymbol{\Theta}_s = \text{vec}(\mathbf{R})$ is an extra parameter vector. Furthermore, the Fisher information matrix (FIM) can be presented as

$$\mathbf{F}(\boldsymbol{\Theta}) = E \left[\left(\frac{\partial \ln f(\mathbf{Z}|\xi, \mathcal{H}_1)}{\partial \boldsymbol{\Theta}^*} \right) \left(\frac{\partial \ln f(\mathbf{Z}|\xi, \mathcal{H}_1)}{\partial \boldsymbol{\Theta}^T} \right) \right], \quad (27)$$

or partitioned as

$$\mathbf{F}(\boldsymbol{\Theta}) = \begin{bmatrix} \mathbf{F}_{\boldsymbol{\Theta}_r, \boldsymbol{\Theta}_r}(\boldsymbol{\Theta}), & \mathbf{F}_{\boldsymbol{\Theta}_r, \boldsymbol{\Theta}_s}(\boldsymbol{\Theta}) \\ \mathbf{F}_{\boldsymbol{\Theta}_s, \boldsymbol{\Theta}_r}(\boldsymbol{\Theta}), & \mathbf{F}_{\boldsymbol{\Theta}_s, \boldsymbol{\Theta}_s}(\boldsymbol{\Theta}) \end{bmatrix}. \quad (28)$$

Next, the statistic of Rao test [48] can be expressed as

$$\Lambda_{Rao} = \frac{\partial \ln f(\mathbf{Z}|\xi, \mathcal{H}_1)}{\partial \boldsymbol{\Theta}_r} \Big|_{\boldsymbol{\Theta}=\hat{\boldsymbol{\Theta}}_0}^T \left[\mathbf{F}^{-1}(\hat{\boldsymbol{\Theta}}_0) \right]_{\boldsymbol{\Theta}_r, \boldsymbol{\Theta}_r} \times \frac{\partial \ln f(\mathbf{Z}|\xi, \mathcal{H}_1)}{\partial \boldsymbol{\Theta}_r^*} \Big|_{\boldsymbol{\Theta}=\hat{\boldsymbol{\Theta}}_0} \underset{\mathcal{H}_0}{\overset{\mathcal{H}_1}{\geq}} \lambda, \quad (29)$$

where $\hat{\boldsymbol{\Theta}}_0 = [\hat{\boldsymbol{\Theta}}_{r_0}^T, \hat{\boldsymbol{\Theta}}_{s_0}^T]^T$ is the MLE of $\boldsymbol{\Theta}$ under \mathcal{H}_0 , and

$$\hat{\boldsymbol{\Theta}}_{r_0} = [0, 0] \quad (30)$$

$$\hat{\boldsymbol{\Theta}}_{s_0} = E \left[\text{vec}(\mathbf{Z}\mathbf{Z}^\dagger + \mathbf{S}) \right] \quad (31)$$

In addition, we have

$$\frac{\partial \ln f(\mathbf{Z}|\xi, \mathcal{H}_1)}{\partial \boldsymbol{\Theta}_r} = \left[\frac{\partial \ln f(\mathbf{Z}|\xi, \mathcal{H}_1)}{\partial \xi_R}, \frac{\partial \ln f(\mathbf{Z}|\xi, \mathcal{H}_1)}{\partial \xi_I} \right]^T, \quad (32)$$

with

$$\frac{\partial \ln f(\mathbf{Z}|\xi, \mathcal{H}_1)}{\partial \xi_R} = 2\text{Re} \left[\boldsymbol{\omega}_D^T(f_d) \mathbf{Z}_1^\dagger \mathbf{R}^{-1} \mathbf{a}_{\text{TR}}(r, \theta) \right], \quad (33)$$

$$\frac{\partial \ln f(\mathbf{Z}|\xi, \mathcal{H}_1)}{\partial \xi_I} = 2\text{Im} \left[\boldsymbol{\omega}_D^T(f_d) \mathbf{Z}_1^\dagger \mathbf{R}^{-1} \mathbf{a}_{\text{TR}}(r, \theta) \right]. \quad (34)$$

Moreover, by resorting to Schuler complementary decomposition theorem [49], $\left[\mathbf{F}^{-1}(\hat{\boldsymbol{\Theta}}_0) \right]_{\boldsymbol{\Theta}_r, \boldsymbol{\Theta}_r}$ can be recast as

$$\left[\mathbf{F}^{-1}(\hat{\boldsymbol{\Theta}}_0) \right]_{\boldsymbol{\Theta}_r, \boldsymbol{\Theta}_r} = \left[\mathbf{F}_{\boldsymbol{\Theta}_r, \boldsymbol{\Theta}_r}(\boldsymbol{\Theta}) - \mathbf{F}_{\boldsymbol{\Theta}_r, \boldsymbol{\Theta}_s}(\boldsymbol{\Theta}) \mathbf{F}_{\boldsymbol{\Theta}_s, \boldsymbol{\Theta}_s}^{-1}(\boldsymbol{\Theta}) \mathbf{F}_{\boldsymbol{\Theta}_s, \boldsymbol{\Theta}_r}(\boldsymbol{\Theta}) \right]^{-1} \Big|_{\boldsymbol{\Theta}=\hat{\boldsymbol{\Theta}}_0}. \quad (35)$$

In this respect, $\mathbf{F}_{\boldsymbol{\Theta}_r, \boldsymbol{\Theta}_r}(\boldsymbol{\Theta})$ can be partitioned as

$$\mathbf{F}_{\boldsymbol{\Theta}_r, \boldsymbol{\Theta}_r}(\boldsymbol{\Theta}) = -E \left[\begin{array}{cc} \frac{\partial^2 \ln f(\mathbf{Z}|\xi, \mathcal{H}_1)}{\partial \xi_R^2}, & \frac{\partial^2 \ln f(\mathbf{Z}|\xi, \mathcal{H}_1)}{\partial \xi_R \partial \xi_I} \\ \frac{\partial^2 \ln f(\mathbf{Z}|\xi, \mathcal{H}_1)}{\partial \xi_I \partial \xi_R}, & \frac{\partial^2 \ln f(\mathbf{Z}|\xi, \mathcal{H}_1)}{\partial \xi_I^2} \end{array} \right] \quad (36)$$

where

$$\frac{\partial^2 \ln f(\mathbf{Z}|\xi, \mathcal{H}_1)}{\partial \xi_R^2} = -2\boldsymbol{\omega}_D^T(f_d) \boldsymbol{\omega}_D^*(f_d) \times \mathbf{a}_{\text{TR}}^\dagger(r, \theta) \mathbf{R}^{-1} \mathbf{a}_{\text{TR}}(r, \theta), \quad (37)$$

$$\frac{\partial^2 \ln f(\mathbf{Z}|\xi, \mathcal{H}_1)}{\partial \xi_I^2} = -2\boldsymbol{\omega}_D^T(f_d) \boldsymbol{\omega}_D^*(f_d) \times \mathbf{a}_{\text{TR}}^\dagger(r, \theta) \mathbf{R}^{-1} \mathbf{a}_{\text{TR}}(r, \theta),$$

$$\frac{\partial^2 \ln f(\mathbf{Z}|\xi, \mathcal{H}_1)}{\partial \xi_I \partial \xi_R} = \frac{\partial^2 \ln f(\mathbf{Z}|\xi, \mathcal{H}_1)}{\partial \xi_R \partial \xi_I} = 0. \quad (38)$$

One can prove that $\mathbf{F}_{\boldsymbol{\Theta}_r, \boldsymbol{\Theta}_s}(\boldsymbol{\Theta}) = \mathbf{0}_{2, \text{MN}}$. Hence, (35) can be recast as

$$\left[\mathbf{F}^{-1}(\hat{\boldsymbol{\Theta}}_0) \right]_{\boldsymbol{\Theta}_r, \boldsymbol{\Theta}_r} = \left[\mathbf{F}_{\boldsymbol{\Theta}_r, \boldsymbol{\Theta}_r}(\boldsymbol{\Theta}) \right]^{-1} \Big|_{\boldsymbol{\Theta}=\hat{\boldsymbol{\Theta}}_0}. \quad (39)$$

Next, taking above derived results into (29) gives the Rao test, as

$$\Lambda_{Rao} = \frac{\left| \mathbf{a}_{\text{TR}}^\dagger(r, \theta) \left(\mathbf{Z}\mathbf{Z}^\dagger + \mathbf{S} \right)^{-1} \mathbf{Z} \boldsymbol{\omega}_D^*(f_d) \right|^2}{\mathbf{a}_{\text{TR}}^\dagger(r, \theta) \left(\mathbf{Z}\mathbf{Z}^\dagger + \mathbf{S} \right)^{-1} \mathbf{a}_{\text{TR}}(r, \theta) \boldsymbol{\omega}_D^T(f_d) \boldsymbol{\omega}_D^*(f_d)} \underset{\mathcal{H}_0}{\overset{\mathcal{H}_1}{\geq}} \lambda, \quad (40)$$

or equivalently

$$\Lambda_{Rao} = \frac{\left| \tilde{\mathbf{a}}^\dagger \left(\mathbf{I} + \tilde{\mathbf{Z}}\tilde{\mathbf{Z}}^\dagger \right)^{-1} \tilde{\mathbf{Z}}_\omega \right|^2}{\tilde{\mathbf{a}}^\dagger \left(\mathbf{I} + \tilde{\mathbf{Z}}\tilde{\mathbf{Z}}^\dagger \right)^{-1} \tilde{\mathbf{a}}} \underset{\mathcal{H}_0}{\overset{\mathcal{H}_1}{\geq}} \lambda. \quad (41)$$

Although the expression for the Rao detector proposed in [39] is similar to (41), the key difference lies in the inverse matrix term $\left(\mathbf{I} + \tilde{\mathbf{Z}}\tilde{\mathbf{Z}}^\dagger \right)$ when $\tilde{\mathbf{Z}}_\omega$ is considered as the received data.

IV. STATISTICAL ANALYSIS

In this section, we will derive closed-form expressions for the PFA and PD of the proposed detectors to facilitate their performance evaluation. Furthermore, during the analysis of Rao detector, the LHAMF detector will be introduced.

A. The PFA and PD of OGLRT

According to the matrix inversion lemma [49], we have

$$\begin{aligned}
& \left(\mathbf{I} + \tilde{\mathbf{Z}}\tilde{\mathbf{Z}}^\dagger \right)^{-1} \\
&= \left(\mathbf{I} + \tilde{\mathbf{Z}}\mathbf{P}_{\omega_{\text{D}}^*(f_d)}^\perp \tilde{\mathbf{Z}}^\dagger + \tilde{\mathbf{Z}}_\omega \tilde{\mathbf{Z}}_\omega^\dagger \right)^{-1} \\
&= \left(\mathbf{I} + \tilde{\mathbf{Z}}\mathbf{P}_{\omega_{\text{D}}^*(f_d)}^\perp \tilde{\mathbf{Z}}^\dagger \right)^{-1} \\
&\quad - \frac{\left(\mathbf{I} + \tilde{\mathbf{Z}}\mathbf{P}_{\omega_{\text{D}}^*(f_d)}^\perp \tilde{\mathbf{Z}}^\dagger \right)^{-1} \tilde{\mathbf{Z}}_\omega \tilde{\mathbf{Z}}_\omega^\dagger \left(\mathbf{I} + \tilde{\mathbf{Z}}\mathbf{P}_{\omega_{\text{D}}^*(f_d)}^\perp \tilde{\mathbf{Z}}^\dagger \right)^{-1}}{1 + \tilde{\mathbf{Z}}_\omega^\dagger \left(\mathbf{I} + \tilde{\mathbf{Z}}\mathbf{P}_{\omega_{\text{D}}^*(f_d)}^\perp \tilde{\mathbf{Z}}^\dagger \right)^{-1} \tilde{\mathbf{Z}}_\omega}.
\end{aligned} \tag{42}$$

Taking (42) into (14), the expression of OGLRT can be recast as

$$\Lambda = \frac{1}{1 - \Lambda'} \underset{\mathcal{H}_0}{\overset{\mathcal{H}_1}{\gtrsim}} \lambda, \tag{43}$$

where

$$\begin{aligned}
\Lambda' &= \frac{\left| \tilde{\mathbf{a}}^\dagger \left(\mathbf{I} + \tilde{\mathbf{Z}}\mathbf{P}_{\omega_{\text{D}}^*(f_d)}^\perp \tilde{\mathbf{Z}}^\dagger \right)^{-1} \tilde{\mathbf{Z}}_\omega \right|^2}{\tilde{\mathbf{a}}^\dagger \left(\mathbf{I} + \tilde{\mathbf{Z}}\mathbf{P}_{\omega_{\text{D}}^*(f_d)}^\perp \tilde{\mathbf{Z}}^\dagger \right)^{-1} \tilde{\mathbf{a}}} \\
&\quad \times \frac{1}{1 + \tilde{\mathbf{Z}}_\omega^\dagger \left(\mathbf{I} + \tilde{\mathbf{Z}}\mathbf{P}_{\omega_{\text{D}}^*(f_d)}^\perp \tilde{\mathbf{Z}}^\dagger \right)^{-1} \tilde{\mathbf{Z}}_\omega}.
\end{aligned} \tag{44}$$

Furthermore, we define (45) as it appears on the first line of the next page.

Since three expressions Λ , Λ' and Λ'' are equivalent [50], the subsequent analysis in this paper primarily focuses on (45). If we let $\tilde{\mathbf{a}}$, $\tilde{\mathbf{Z}}_\omega$, and $\mathbf{I} + \tilde{\mathbf{Z}}\mathbf{P}_{\omega_{\text{D}}^*(f_d)}^\perp \tilde{\mathbf{Z}}^\dagger$ denote the steering vector, received data, and SCM, respectively, the detector represented by (45) is formally consistent with the KGLRT. In addition, the term $\tilde{\mathbf{a}}^\dagger \left(\mathbf{I} + \tilde{\mathbf{Z}}\mathbf{P}_{\omega_{\text{D}}^*(f_d)}^\perp \tilde{\mathbf{Z}}^\dagger \right)^{-1} \tilde{\mathbf{Z}}_\omega$ can be further rewritten as

$$\tilde{\mathbf{a}}^\dagger \left(\mathbf{I} + \tilde{\mathbf{Z}}\mathbf{P}_{\omega_{\text{D}}^*(f_d)}^\perp \tilde{\mathbf{Z}}^\dagger \right)^{-1} \tilde{\mathbf{Z}}_\omega = \frac{\mathbf{a}_{\text{TR}}^\dagger(r, \theta) \mathbf{S}_+^{-1} \mathbf{Z} \omega_{\text{D}}^*(f_d)}{\sqrt{\omega_{\text{D}}^T(f_d) \omega_{\text{D}}^*(f_d)}}, \tag{46}$$

with

$$\mathbf{S}_+ = \mathbf{S} + \mathbf{Z}\mathbf{P}_{\omega_{\text{D}}^*(f_d)}^\perp \mathbf{Z}^\dagger. \tag{47}$$

Next, our focus can turn on the term \mathbf{S}_+ .

Theorem 1. *Under \mathcal{H}_0 hypothesis, \mathbf{S}_+ obeys a complex Wishart distribution with degrees of freedom (DoFs) being $(L+1)K$, and MN and covariance matrix being \mathbf{R} .*

Proof. One can easily prove that [51]

$$\mathbf{S} \sim CW(LK, MN; \mathbf{R}). \tag{48}$$

Furthermore, based on the results from Appendix A in [44], each column of $\mathbf{Z}\mathbf{P}_{\omega_{\text{D}}^*(f_d)}^\perp \in \mathbb{C}^{MN \times K}$ is zero-mean Gaussian vector with covariance matrix \mathbf{R} , namely $\left[\mathbf{Z}\mathbf{P}_{\omega_{\text{D}}^*(f_d)}^\perp \right]_k \sim \mathcal{CN}(0, \mathbf{R})$, $k = 1, 2, \dots, K$ under \mathcal{H}_0 hypothesis.

Due to $\mathbf{Z}\mathbf{P}_{\omega_{\text{D}}^*(f_d)}^\perp \left(\mathbf{P}_{\omega_{\text{D}}^*(f_d)}^\perp \right)^\dagger \mathbf{Z}^\dagger = \mathbf{Z}\mathbf{P}_{\omega_{\text{D}}^*(f_d)}^\perp \mathbf{Z}^\dagger$, we have

$$\mathbf{Z}\mathbf{P}_{\omega_{\text{D}}^*(f_d)}^\perp \mathbf{Z}^\dagger \sim CW(K, MN; \mathbf{R}). \tag{49}$$

By resorting to the result of [Theorem 7.3.2] [52], one can easily obtain that

$$\mathbf{S}_+ \sim CW((L+1)K, MN; \mathbf{R}). \tag{50}$$

□

Despite [37] stating that \mathbf{S}_+ follows a complex Wishart distribution, the DoFs provided are incorrect.

Based on the analysis above, we can further derive that

$$\Lambda'' \sim \begin{cases} C\mathcal{F}_{1, MM-1} & \text{under } \mathcal{H}_0, \\ C\mathcal{F}_{1, MM-1}(\alpha\mathcal{B}) & \text{under } \mathcal{H}_1, \end{cases} \tag{51}$$

where $MM = (L+1)K - MN + 1$ and $\alpha\mathcal{B}$ denote the DoFs and the non-central parameter, respectively, with

$$\alpha = |\xi|^2 \omega_{\text{D}}^T(f_d) \omega_{\text{D}}^*(f_d) \mathbf{a}_{\text{TR}}^\dagger(r, \theta) \mathbf{R}^{-1} \mathbf{a}_{\text{TR}}(r, \theta). \tag{52}$$

Moreover, \mathcal{B} follows the central complex Beta distribution, i.e.,

$$\mathcal{B} \sim \begin{cases} C\beta_{MM+1, MN-1} & \text{under } \mathcal{H}_0 \\ C\beta_{MM+1, MN-1} & \text{under } \mathcal{H}_1 \end{cases}. \tag{53}$$

Further, the PDF of \mathcal{B} is

$$\begin{aligned}
f_{\mathcal{B}}(\mathcal{B}) &= f_{\mathcal{B}|\mathcal{H}_0}(\mathcal{B}) = f_{\mathcal{B}|\mathcal{H}_1}(\mathcal{B}) \\
&= \frac{\mathcal{B}^{MM} (1 - \mathcal{B})^{MN-2}}{\beta(MM+1, MN-1)}.
\end{aligned} \tag{54}$$

Therefore, (51) shows that OGLRT own the CFAR property against the covariance matrix under \mathcal{H}_0 hypothesis.

Next, by using the results [47], [53], the expression for the PFA of OGLRT can be written as

$$\text{PFA} = (1 + \lambda)^{-MM} \tag{55}$$

Finally, we have

$$P_{\text{D}} = \int_0^1 [1 - \mathcal{P}_{\mathcal{H}_1, \mathcal{B}}(\lambda)] f_{\mathcal{B}}(\mathcal{B}) d\mathcal{B}, \tag{56}$$

with

$$\mathcal{P}_{\mathcal{H}_1, \mathcal{B}}(\gamma) = \sum_{i=0}^{MM-1} C_{\text{MM}}^{1+i} \frac{\gamma^{1+i}}{(1+\gamma)^{\text{MM}}} \text{IG}_{i+1} \left(\frac{\alpha\mathcal{B}}{1+\gamma} \right). \tag{57}$$

The notation $\text{IG}_{\ell+1}(\mathbf{h})$ stands for the incomplete gamma function, given by

$$\text{IG}_{\ell+1}(\mathbf{h}) = \exp(-\mathbf{h}) \sum_{j=0}^{\ell} \frac{1}{\Gamma(j+1)} \mathbf{h}^j \tag{58}$$

B. The PFA and PD of TGLRT

In this section, we will derive closed-form expressions for the PFA and PD of the TGLRT detector. For the TGLRT detector in (24), its detection statistic expression is consistent with the detector in [41]. For the threshold of the TGLRT detector, it is only necessary to rewrite the λ in (55) as $\lambda\mathcal{B}$. In other words, according to the results in [41], the relationship

$$\begin{aligned}
\Lambda'' &= \frac{\Lambda'}{1 - \Lambda'} \\
&= \frac{\left| \tilde{\mathbf{a}}^\dagger \left(\mathbf{I} + \tilde{\mathbf{Z}} \mathbf{P}_{\omega_{\mathbb{D}}^*(f_d)}^\perp \tilde{\mathbf{Z}}^\dagger \right)^{-1} \tilde{\mathbf{Z}}_\omega \right|^2 / \tilde{\mathbf{a}}^\dagger \left(\mathbf{I} + \tilde{\mathbf{Z}} \mathbf{P}_{\omega_{\mathbb{D}}^*(f_d)}^\perp \tilde{\mathbf{Z}}^\dagger \right)^{-1} \tilde{\mathbf{a}}}{1 + \tilde{\mathbf{Z}}_\omega^\dagger \left(\mathbf{I} + \tilde{\mathbf{Z}} \mathbf{P}_{\omega_{\mathbb{D}}^*(f_d)}^\perp \tilde{\mathbf{Z}}^\dagger \right)^{-1} \tilde{\mathbf{Z}}_\omega - \frac{\left| \tilde{\mathbf{a}}^\dagger \left(\mathbf{I} + \tilde{\mathbf{Z}} \mathbf{P}_{\omega_{\mathbb{D}}^*(f_d)}^\perp \tilde{\mathbf{Z}}^\dagger \right)^{-1} \tilde{\mathbf{Z}}_\omega \right|^2}{\tilde{\mathbf{a}}^\dagger \left(\mathbf{I} + \tilde{\mathbf{Z}} \mathbf{P}_{\omega_{\mathbb{D}}^*(f_d)}^\perp \tilde{\mathbf{Z}}^\dagger \right)^{-1} \tilde{\mathbf{a}}}},
\end{aligned} \tag{45}$$

between the detection threshold of TGLRT and PFA can be expressed as:

$$PFA = \int_0^1 \frac{1}{(1 + \lambda \mathcal{B}_1)^{MM_1}} f_{\mathcal{B}_1}(\mathcal{B}_1) d\mathcal{B}_1, \tag{59}$$

where $MM_1 = LK - MN + 1$ and $\mathcal{B}_1 \sim C\beta_{MM_1, MN-1}$. The PDF of \mathcal{B}_1 , denoted as $f_{\mathcal{B}_1}(\mathcal{B}_1)$, can be obtained by replacing the degrees of freedom MM in (54) with MM_1 . Obviously, TGLRT possesses the CFAR property due to the reason that the PFA expression (59) is irrelevant with the covariance matrix.

Additionally, the PD can be expressed as

$$P_D = \int_0^1 [1 - \mathcal{P}_{\mathcal{H}_1, \mathcal{B}_1}(\lambda \mathcal{B}_1)] f_{\mathcal{B}_1}(\mathcal{B}_1) d\mathcal{B}_1. \tag{60}$$

After substituting MM_1 for MM in (57), we can obtain the expression for $\mathcal{P}_{\mathcal{H}_1, \mathcal{B}_1}(\gamma)$.

C. The PFA and PD of Rao

Using (42), the denominator of (41) can be recast as

$$\begin{aligned}
\tilde{\mathbf{a}}^\dagger \left(\mathbf{I} + \tilde{\mathbf{Z}} \tilde{\mathbf{Z}}^\dagger \right)^{-1} \mathbf{a} &= \tilde{\mathbf{a}}^\dagger \left(\mathbf{I} + \tilde{\mathbf{Z}} \mathbf{P}_{\omega_{\mathbb{D}}^*(f_d)}^\perp \tilde{\mathbf{Z}}^\dagger \right)^{-1} \mathbf{a} \\
&- \frac{\left| \tilde{\mathbf{a}}^\dagger \left(\mathbf{I} + \tilde{\mathbf{Z}} \mathbf{P}_{\omega_{\mathbb{D}}^*(f_d)}^\perp \tilde{\mathbf{Z}}^\dagger \right)^{-1} \tilde{\mathbf{Z}}_\omega \right|^2}{1 + \tilde{\mathbf{Z}}_\omega^\dagger \left(\mathbf{I} + \tilde{\mathbf{Z}} \mathbf{P}_{\omega_{\mathbb{D}}^*(f_d)}^\perp \tilde{\mathbf{Z}}^\dagger \right)^{-1} \tilde{\mathbf{Z}}_\omega}.
\end{aligned} \tag{61}$$

Besides, the numerator of (41) can be simplified as

$$\begin{aligned}
&\left| \tilde{\mathbf{a}}^\dagger \left(\mathbf{I} + \tilde{\mathbf{Z}} \tilde{\mathbf{Z}}^\dagger \right)^{-1} \tilde{\mathbf{Z}}_\omega \right|^2 \\
&= \frac{\left| \tilde{\mathbf{a}}^\dagger \left(\mathbf{I} + \tilde{\mathbf{Z}} \mathbf{P}_{\omega_{\mathbb{D}}^*(f_d)}^\perp \tilde{\mathbf{Z}}^\dagger \right)^{-1} \tilde{\mathbf{Z}}_\omega \right|^2}{\left| 1 + \tilde{\mathbf{Z}}_\omega^\dagger \left(\mathbf{I} + \tilde{\mathbf{Z}} \mathbf{P}_{\omega_{\mathbb{D}}^*(f_d)}^\perp \tilde{\mathbf{Z}}^\dagger \right)^{-1} \tilde{\mathbf{Z}}_\omega \right|^2}.
\end{aligned} \tag{62}$$

Applying (61) and (62), after some algebra, Rao detector expression can be rewritten as (63) (which is shown on the first line of next page) or equivalently

$$\Lambda_{Rao} = \frac{\Lambda' \Lambda''}{\Lambda_{LHAMF}} \underset{\mathcal{H}_0}{\overset{\mathcal{H}_1}{\geq}} \lambda, \tag{64}$$

where the definition of Λ_{LHAMF} is

$$\Lambda_{LHAMF} = \frac{\left| \tilde{\mathbf{a}}^\dagger \left(\mathbf{I} + \tilde{\mathbf{Z}} \mathbf{P}_{\omega_{\mathbb{D}}^*(f_d)}^\perp \tilde{\mathbf{Z}}^\dagger \right)^{-1} \tilde{\mathbf{Z}}_\omega \right|^2}{\tilde{\mathbf{a}}^\dagger \left(\mathbf{I} + \tilde{\mathbf{Z}} \mathbf{P}_{\omega_{\mathbb{D}}^*(f_d)}^\perp \tilde{\mathbf{Z}}^\dagger \right)^{-1} \tilde{\mathbf{a}}}. \tag{65}$$

It is worth noting that if we define the steering vector, received data, and SCM as $\tilde{\mathbf{a}}$, $\tilde{\mathbf{Z}}_\omega$, $\left(\mathbf{I} + \tilde{\mathbf{Z}} \mathbf{P}_{\omega_{\mathbb{D}}^*(f_d)}^\perp \tilde{\mathbf{Z}}^\dagger \right)$ respectively, then (65) is the corresponding TGLRT detector, which is also identical in form to the AMF detector in reference [41]. In order to distinguish the detector represented by (65) from the previous TGLRT detector in the text, this paper defines it as the LHAMF detector¹.

In contrast to TGLRT, the LHAMF detector utilizes both training and test data for covariance matrix estimation, potentially leading to slightly better performance. Additionally, by changing the degrees of freedom in (59) and (60) from MM_1 to MM, the expressions for PFA and PD of the LHAMF detector can be derived, i.e.,

$$PFA = \int_0^1 \frac{1}{(1 + \lambda \mathcal{B})^{MM}} f_{\mathcal{B}}(\mathcal{B}) d\mathcal{B} \tag{66}$$

and

$$P_D = \int_0^1 [1 - \mathcal{P}_{\mathcal{H}_1, \mathcal{B}}(\lambda \mathcal{B})] f_{\mathcal{B}}(\mathcal{B}) d\mathcal{B}. \tag{67}$$

Define

$$\mathcal{B} = \frac{\Lambda''}{\Lambda_{LHAMF}}. \tag{68}$$

Note that referring to the result in [39], the distribution of random variables presented in (68) aligns with (53). Hence, we adopt the same variable symbol. Subsequently, the expression for the Rao detector can be given by

$$\Lambda = \frac{\mathcal{B} \Lambda''}{1 + \Lambda''} \underset{\mathcal{H}_0}{\overset{\mathcal{H}_1}{\geq}} \lambda. \tag{69}$$

Similar to [39], the PFA for Rao detector can be expressed as

$$PFA = (1 - \lambda)^{(L+1)K-1}. \tag{70}$$

Eq.(70) implies that there is no covariance matrix term in the expression of PFA for Rao detector. Above result further indicates that Rao detector exhibit CFAR property against noise covariance matrix under \mathcal{H}_0 hypothesis.

Furthermore, the detection probability can be expressed as

$$P_D = \int_\lambda^1 \left[1 - \mathcal{P}_{\mathcal{H}_1, \mathcal{B}} \left(\frac{\lambda}{\mathcal{B} - \lambda} \right) \right] f_{\mathcal{B}}(\mathcal{B}) d\mathcal{B} \tag{71}$$

Finally, for the convenience of readers, Table I provides the PD and PFA for detectors above mentioned.

¹“LH” represents the first letters of the surnames of the first two authors.

$$\begin{aligned}
A_{Rao} = & \frac{\left| \tilde{\mathbf{a}}^\dagger \left(\mathbf{I} + \tilde{\mathbf{Z}} \mathbf{P}_{\omega_{\text{D}}^*(f_d)}^\perp \tilde{\mathbf{Z}}^\dagger \right)^{-1} \tilde{\mathbf{Z}}_\omega \right|^2}{\left(1 + \tilde{\mathbf{Z}}_\omega^\dagger \left(\mathbf{I} + \tilde{\mathbf{Z}} \mathbf{P}_{\omega_{\text{D}}^*(f_d)}^\perp \tilde{\mathbf{Z}}^\dagger \right)^{-1} \tilde{\mathbf{Z}}_\omega \right) \tilde{\mathbf{a}}^\dagger \left(\mathbf{I} + \tilde{\mathbf{Z}} \mathbf{P}_{\omega_{\text{D}}^*(f_d)}^\perp \tilde{\mathbf{Z}}^\dagger \right)^{-1} \mathbf{a}} \\
& \times \frac{1}{1 + \tilde{\mathbf{Z}}_\omega^\dagger \left(\mathbf{I} + \tilde{\mathbf{Z}} \mathbf{P}_{\omega_{\text{D}}^*(f_d)}^\perp \tilde{\mathbf{Z}}^\dagger \right)^{-1} \tilde{\mathbf{Z}}_\omega - \frac{\left| \tilde{\mathbf{a}}^\dagger \left(\mathbf{I} + \tilde{\mathbf{Z}} \mathbf{P}_{\omega_{\text{D}}^*(f_d)}^\perp \tilde{\mathbf{Z}}^\dagger \right)^{-1} \tilde{\mathbf{Z}}_\omega \right|^2}{\tilde{\mathbf{a}}^\dagger \left(\mathbf{I} + \tilde{\mathbf{Z}} \mathbf{P}_{\omega_{\text{D}}^*(f_d)}^\perp \tilde{\mathbf{Z}}^\dagger \right)^{-1} \mathbf{a}}}
\end{aligned} \tag{63}$$

TABLE I
THE STATISTICAL EXPRESSIONS, PD AND PFA FOR PROPOSED DETECTORS.

| | OGLRT | TGLRT | LHAMF | Rao |
|------------------------|-------|-------|-------|------|
| Statistical expression | (14) | (24) | (65) | (41) |
| PFA | (55) | (59) | (66) | (70) |
| P_D | (56) | (60) | (67) | (71) |

V. SIMULATION RESULTS

This section will verify the derived theory's correctness through numerical simulation. The parameters are set as follows: $M = 4$, $N = 3$ are the number of transmit and receive elements, respectively. The carrier frequency is $f_0 = 2$ GHz, and the frequency offset between the elements equals the signal bandwidth, i.e., $B = \Delta f = 1$ MHz, and Doppler frequency shift is $f_d = 0.2$. $d_T = d_R = \frac{c}{2f_0}$ represent the distance between the transmit and receive elements. Further, the Signal-to-Jamming-Plus-Noise Ratio (SJNR) is defined as

$$\mathbf{R} = \sigma_c^2 \left(\sum_d \sigma_{\text{jam},d}^2 \mathbb{R}_d + \sum_u \sigma_{\text{sup},u}^2 \mathbb{R}_u + \mathbf{I} \right), \tag{72}$$

$\sigma_{\text{jam},d}^2$ and $\sigma_{\text{sup},u}^2$ represents the power of the d th deception jamming signal and the u th suppression jamming. \mathbb{R}_d and \mathbb{R}_u denote the covariance matrix of deceptive jamming and suppressive jamming, respectively. They are defined as

$$\begin{aligned}
\mathbb{R}_d &= \mathbf{a}_{\text{TR}}(r_d, \theta_d) \mathbf{a}_{\text{TR}}^\dagger(r_d, \theta_d) \\
\mathbb{R}_u &= \mathbf{1}_{M \times M} \otimes \left[\mathbf{a}_R(\theta_u) \mathbf{a}_R^\dagger(\theta_u) \right]
\end{aligned} \tag{73}$$

where $\mathbf{1}_{M \times M}$ is a matrix with all 1 elements, σ_c^2 and \mathbf{I} represent the power and covariance matrix of noise, respectively. In addition, $\delta_{\text{jam}} = 10 \log \frac{\sum_d \sigma_{\text{jam},d}^2}{\sigma_c^2}$ and $\delta_{\text{sup}} = 10 \log \frac{\sum_u \sigma_{\text{sup},u}^2}{\sigma_c^2}$ represent jamming to noise ratio (JNR) for deception jamming and suppression jamming. At the same time, signal to noise ratio (SNR) is defined as $\text{SNR} = 10 \log \frac{|\epsilon|^2}{\sigma_n^2}$. The target is located in $(r, \theta) = (15.12 \text{ Km}, 30^\circ)$, two deceptive targets located $(r_1, \theta_1) = (15.165 \text{ Km}, 30^\circ)$, $(r_2, \theta_2) = (30.48 \text{ Km}, 28^\circ)$, and $\delta_{\text{jam},1} = \delta_{\text{jam},2} = 20$ dB, respectively, and one suppressive jammer with JNR of $\delta_{\text{sup}} = 30$ dB and the angle is $\theta_u = -20^\circ$. The detection threshold and PD obtained by $\frac{100}{\text{PFA}}$ and 10^4 independent Monte Carlo (MC) trials, respectively, where $\text{PFA} = 10^{-3}$.

Additionally, for cross-validation purposes, we compared the performance of the statistical expressions with the expressions for PFA and PD. It is worth noting that the experimental results obtained from MC and statistical equivalent expressions are marked as "MC" and "TH", respectively.

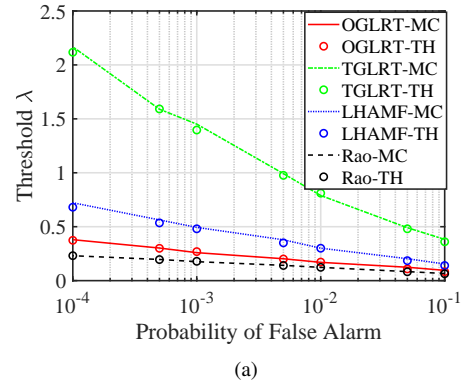


Fig. 1. The detection threshold of the proposed detectors varies with the false alarm probability.

Fig.1 shows the variation curves of the detection threshold of the proposed detectors with respect to the false alarm rate PFA. The lines represent the experimental results obtained through MC simulations, while the symbols \circ represent the theoretical values obtained using the expressions in the second row of Table I. It can be observed from the figure that the theoretical values closely match the results obtained from MC simulations, indicating the correctness of the theoretical derivations in this section.

Under different numbers of training data and snapshots, Fig.2 presents the PDs versus SJNR for proposed detectors. The agreement between the MC simulations and theoretical predictions in Fig.2 validates the correctness of the prior theoretical analysis. In Fig.2 (a), where training data is limited, the alignment between MC and theoretical results for OGLRT is weaker compared to Fig.2 (b) with more training data. Additionally, Fig.2 (a) reveals OGLRT's superior performance under the given simulation conditions, while TGLRT performs the poorest, and LHAMF outperforms TGLRT. Comparing Fig.2 (a) and Fig.2 (b), it becomes evident that having more training data enhances detector performance under the same number of snapshots, allowing for more accurate covariance matrix estimation. Comparing Fig.2 (b) and Fig.2 (c) suggests that, with limited training data, increasing the number of snap-

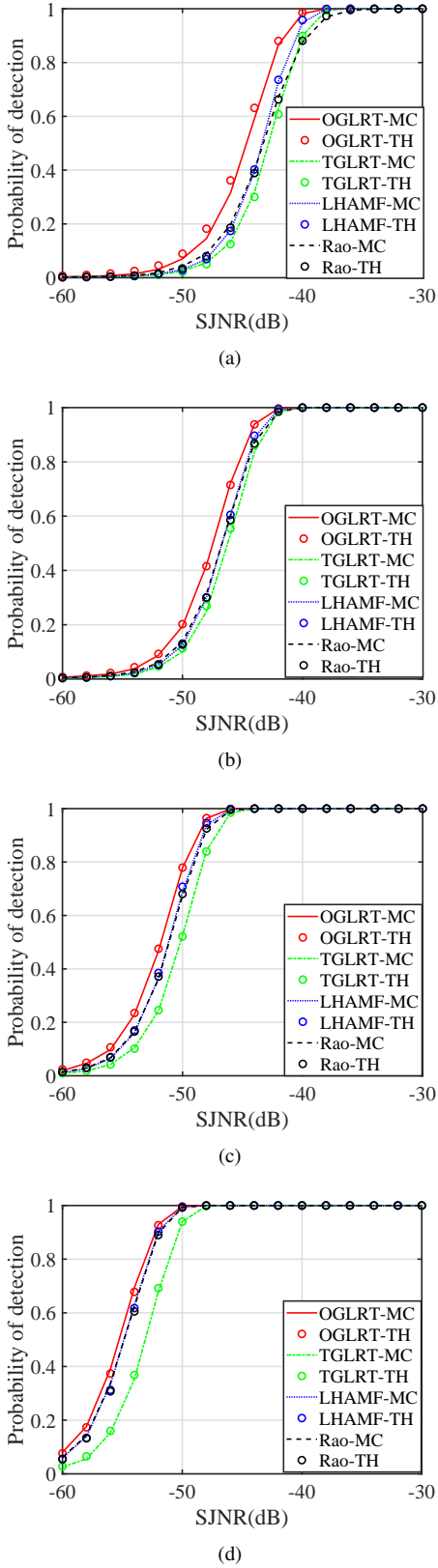


Fig. 2. The curves of PD versus SJNR under different number of training data and snapshots. (a) $L=4$, $K=6$, (b) $L=6$, $K=6$, (c) $L=2$, $K=16$, (d) $L=1$, $K=32$.

shots also improves the detection performance. In both cases, the data used for covariance matrix estimation already exceeds $2MN$. Thus, enhancing the accuracy of covariance matrix estimation through increased training data yields marginal improvements. However, in this scenario, increasing the number of snapshots significantly enhances detection performance by improving covariance estimation accuracy, as demonstrated in Fig.2 (d).

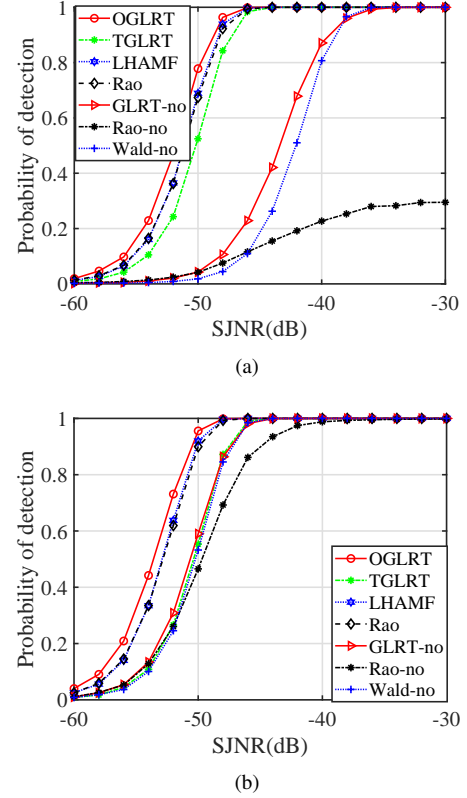


Fig. 3. The curves of PD with and without training data versus SJNR (a) $L=2$, $K=16$, (b) $L=1$, $K=24$.

To further demonstrate the impact of training data on detector performance, three detectors without training data, namely GLRT-no, Rao-no, and Wald-no, are introduced as comparative detectors, expressed as [12], [46]

$$\Lambda_{GLRT-no} = \frac{\mathbf{a}_{TR}^\dagger(r, \theta) \left(\mathbf{Z} \mathbf{P}_D^\perp(f_d) \mathbf{Z}^\dagger \right)^{-1} \mathbf{a}_{TR}(r, \theta)}{\mathbf{a}_{TR}^\dagger(r, \theta) \left(\tilde{\mathbf{Z}} \tilde{\mathbf{Z}}^\dagger \right)^{-1} \mathbf{a}_{TR}(r, \theta)} \underset{\mathcal{H}_0}{\overset{\mathcal{H}_1}{\geq}} \lambda, \quad (74)$$

$$\Lambda_{Rao-no} = \frac{\left| \mathbf{a}_{TR}^\dagger(r, \theta) \left(\mathbf{Z} \mathbf{Z}^\dagger \right)^{-1} \mathbf{Z} \omega_D^*(f_d) \right|^2}{\mathbf{a}_{TR}^\dagger(r, \theta) \left(\mathbf{Z} \mathbf{Z}^\dagger \right)^{-1} \mathbf{a}_{TR}(r, \theta) \omega_D^T(f_d) \omega_D^*(f_d)} \underset{\mathcal{H}_0}{\overset{\mathcal{H}_1}{\geq}} \lambda, \quad (75)$$

$$\Lambda_{Wald-no} = \frac{\left| \mathbf{a}_{TR}^\dagger(r, \theta) \left(\mathbf{Z} \mathbf{P} \omega_D^*(f_d) \mathbf{Z}^\dagger \right)^{-1} \mathbf{Z} \omega_D^*(f_d) \right|^2}{\mathbf{a}_{TR}^\dagger(r, \theta) \left(\mathbf{Z} \mathbf{P} \omega_D^*(f_d) \mathbf{Z}^\dagger \right)^{-1} \mathbf{a}_{TR}(r, \theta) \omega_D^T(f_d) \omega_D^*(f_d)}$$

$$\underset{\mathcal{H}_0}{\overset{\mathcal{H}_1}{\gtrless}} \lambda. \quad (76)$$

Fig. 3 compares the performance of the proposed detectors with those lacking training data with $L = 2, K = 16$, and $L = 1, K = 24$. In Fig. 3 (a), it is evident that the performance of the Rao detector without training data is the poorest with fewer snapshots. This result is expected, given that the smaller value of K hampers the acquisition of an accurate covariance matrix. Contrastingly, with the support of training data, the proposed detectors demonstrate the ability to detect targets even with a limited number of snapshots, showcasing notably superior performance compared to detectors without training data. In Fig. 3 (b), it is demonstrated that even with a more significant number of snapshots, the performance of the three detectors without training data remains inferior to the proposed detectors, which benefit from training data.

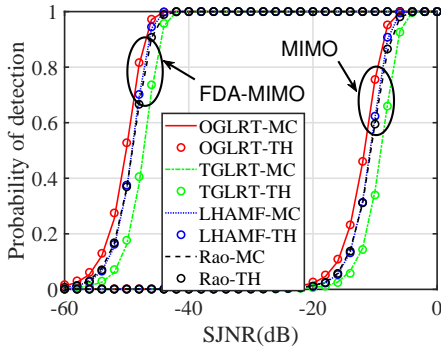
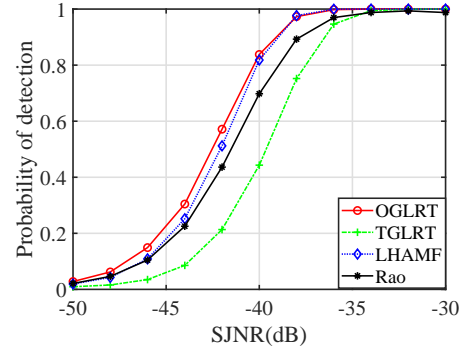


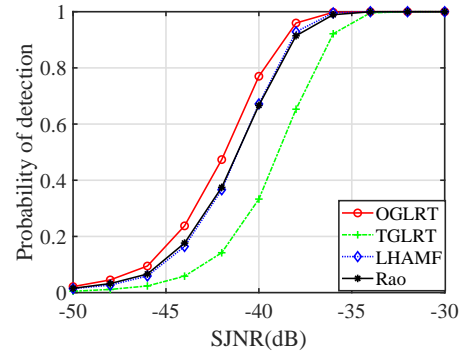
Fig. 4. Comparison of detection performance of the proposed detectors for FDA-MIMO and MIMO radars, where $L = 2, K = 12$.

Furthermore, by setting the frequency offset $\Delta f = 0$ in the transmitting-receiving steering vector of FDA-MIMO radar, we obtain the transmitting-receiving steering vector for MIMO radar. For the detection problem discussed in this paper, Fig. 4 presents the PDs versus SJNR for FDA-MIMO and MIMO radar when $L = 2$ and $K = 12$. The results in Fig. 4 indicate that the detectors proposed in this paper and the corresponding statistical equivalent theory also apply to MIMO radar. In other words, the MC results for MIMO radar align well with the theoretical predictions. Specifically, OGLRT exhibits the best performance, LHAMF and Rao detectors perform nearly identically, and TGLRT demonstrates the poorest performance. Additionally, under the given parameters, the PD of FDA-MIMO radar significantly outperforms that of MIMO radar.

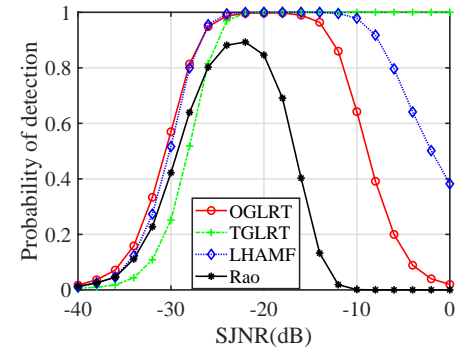
However, in practice, due to the errors in array calibration, waveform mismatch, and so on, the actual signal steering vector does not fully match the nominal one [51], [54], [55]. To measure the error, we define φ represent the angle between actual and nominal steering vector, the degree of mismatch can



(a)



(b)



(c)

Fig. 5. PD versus SJNR when the signal mismatch, where $L = 1, K = 24$. (a) $\cos^2 \varphi = 0.76$, (b) $\cos^2 \Phi = 0.76$, (c) $\cos^2 \varphi = 0.76, \cos^2 \Phi = 0.76$.

be written as [42], [43], [56], [57]

$$\cos^2 \varphi = \frac{\mathbf{a}_{TR}^\dagger(r, \theta) \mathbf{R}^{-1} \mathbf{a}_{TR}(r_0, \theta_0)}{\mathbf{a}_{TR}^\dagger(r, \theta) \mathbf{R}^{-1} \mathbf{a}_{TR}(r, \theta)} \times \frac{\mathbf{a}_{TR}^\dagger(r_0, \theta_0) \mathbf{R}^{-1} \mathbf{a}_{TR}(r, \theta)}{\mathbf{a}_{TR}^\dagger(r_0, \theta_0) \mathbf{R}^{-1} \mathbf{a}_{TR}(r_0, \theta_0)}, \quad (77)$$

where, $\mathbf{a}_{TR}^\dagger(r, \theta)$ and $\mathbf{a}_{TR}(r_0, \theta_0)$ represent the actual and nominal transmitting-receiving steering vector, respectively. Similarly, to measure the signal mismatch in the Doppler dimension, we have

$$\cos^2 \Phi = \frac{\left| \omega_D^\dagger(f_{d,0}) \omega_D(f_d) \right|^2}{\left\| \omega_D^\dagger(f_{d,0}) \right\|^2 \left\| \omega_D(f_d) \right\|^2}, \quad (78)$$

where $\omega_D(f_{d,0})$ and $\omega_D(f_d)$ are the actual and nominal Doppler steering vector, respectively.

Regarding mismatched signals with $L = 1$ and $K = 24$, Fig.5 illustrates the PDs of the proposed detectors against SJNR. In Fig.5 (a), when there is no error in the Doppler dimension and only mistakes in the transmitting-receiving steering vector that cause signal mismatch, it is evident that signal mismatch significantly degrades detection performance. OGLRT exhibits the best performance in this scenario, while TGLRT's performance remains poor. Furthermore, Fig.5 (b) considers only signal mismatch in the Doppler dimension², resulting in more significant performance degradation compared to Fig.5 (a). Finally, in Fig.5 (c), considering signal mismatch in both the transmitting-receiving steering vector and Doppler dimensions, the PDs for three detectors, except TGLRT, are not a single-valued function of SJNR. At low SJNR, the performance of LHAMF and OGLRT is similar and slightly better than the other two detectors. In contrast, at high SJNR, TGLRT exhibits the best detection performance, followed by LHAMF, while the performance of the Rao detector is poor and may not even work.

In summary, under no signal mismatch or only slight mismatch, the OGLRT detector is recommended, and TGLRT should be the last choice. However, in the presence of significant signal errors, TGLRT emerges as the most robust choice.

VI. CONCLUSION

This study delves into the detection of a moving target in Gaussian noise with an unknown covariance matrix using FDA-MIMO radar, introducing four adaptive detectors: OGLRT, TGLRT, Rao, and LHAMF. Closed-form expressions for the PFA and PD, along with confirmation of CFAR properties, are provided. Simulation results highlight the improved performance obtained by leveraging training data for covariance matrix estimation. The mismatch in the Doppler dimension has a more pronounced impact on detector performance compared to the mismatch in the transmitting-receiving steering vector. We recommend selecting the optimal detector based on the level of signal mismatch. OGLRT is preferable in scenarios with signal matching or slight mismatch, while TGLRT exhibits robust performance in cases of significant signal mismatch. FDA-MIMO radar demonstrates significant advantages over traditional MIMO in Gaussian noise environments with deceptive mainlobe jamming. The closed-form expressions for PFA and PD in the presence of Doppler signal mismatch can serve as a direction for future research.

²In deriving the statistical expression, the signal mismatch was not considered. This is because no available literature incorporates signal mismatch in the Doppler dimension into consideration, and the authors believe this is a topic worth investigating in future research. Therefore, the results presented in Fig.5 are all obtained through MC simulations.

APPENDIX

A. OGLRT

Resorting to one-step GLRT [47] criterion, the OGLRT detector can be given by

$$\Lambda = \frac{\max_{\xi, \mathbf{R}} f(\mathbf{Z}, \mathbf{Y} | \xi, \mathbf{R}, \mathcal{H}_1)}{\max_{\mathbf{R}} f(\mathbf{Z}, \mathbf{Y} | \mathbf{R}, \mathcal{H}_0)} \underset{\mathcal{H}_0}{\overset{\mathcal{H}_1}{\geq}} \lambda. \quad (79)$$

According to (11), the MLE of \mathbf{R} under \mathcal{H}_1 is

$$\hat{\mathbf{R}}_1 = \frac{\mathbf{Z}_1 \mathbf{Z}_1^\dagger + \mathbf{S}}{K(L+1)}. \quad (80)$$

Define

$$\tilde{\mathbf{Z}} = \mathbf{S}^{-1/2} \mathbf{Z}, \quad (81)$$

$$\tilde{\mathbf{a}} = \mathbf{S}^{-1/2} \mathbf{a}_{\text{TR}}(r, \theta). \quad (82)$$

Inserting (80) into (11), result in

$$\begin{aligned} f(\mathbf{Z}, \mathbf{Y} | \xi, \hat{\mathbf{R}}_1, \mathcal{H}_1) &= \frac{\text{cont.}}{\det^{K(L+1)}(\mathbf{Z}_1 \mathbf{Z}_1^\dagger + \mathbf{S})} \\ &= \frac{\text{cont.}}{\det^{K(L+1)}(\mathbf{S}) [\mathcal{G}(\xi)]^{K(L+1)}}. \end{aligned} \quad (83)$$

where

$$\begin{aligned} \mathcal{G}(\xi) &= \det \left[\mathbf{I} + \left(\tilde{\mathbf{Z}} - \xi \tilde{\mathbf{a}} \omega_D^T(f_d) \right) \left(\tilde{\mathbf{Z}} - \xi \tilde{\mathbf{a}} \omega_D^T(f_d) \right)^\dagger \right] \\ &= \det \left[\mathbf{I} + \tilde{\mathbf{Z}} \mathbf{P}_{\omega_D^*(f_d)}^\perp \tilde{\mathbf{Z}}^\dagger \right] \det \left[\mathbf{I} + \omega_D^T(f_d) \omega_D^*(f_d) \right] \\ &\quad \times \left(\xi \tilde{\mathbf{a}} - \frac{\tilde{\mathbf{Z}} \omega_D^*(f_d)}{\omega_D^T(f_d) \omega_D^*(f_d)} \right) \left(\xi \tilde{\mathbf{a}} - \frac{\tilde{\mathbf{Z}} \omega_D^*(f_d)}{\omega_D^T(f_d) \omega_D^*(f_d)} \right)^\dagger \\ &= \det \left[\mathbf{I} + \tilde{\mathbf{Z}} \mathbf{P}_{\omega_D^*(f_d)}^\perp \tilde{\mathbf{Z}}^\dagger \right] h(\xi), \end{aligned} \quad (84)$$

and

$$\begin{aligned} h(\xi) &= 1 + \omega_D^T(f_d) \omega_D^*(f_d) \left(\xi \tilde{\mathbf{a}} - \frac{\tilde{\mathbf{Z}} \omega_D^*(f_d)}{\omega_D^T(f_d) \omega_D^*(f_d)} \right)^\dagger \\ &\quad \times \left(\mathbf{I} + \tilde{\mathbf{Z}} \mathbf{P}_{\omega_D^*(f_d)}^\perp \tilde{\mathbf{Z}}^\dagger \right)^{-1} \left(\xi \tilde{\mathbf{a}} - \frac{\tilde{\mathbf{Z}} \omega_D^*(f_d)}{\omega_D^T(f_d) \omega_D^*(f_d)} \right). \end{aligned} \quad (85)$$

To find the MLE of ξ in (83), taking (85) w.r.t. ξ , yields

$$\begin{aligned} \frac{\partial h(\xi)}{\partial \xi} &= \omega_D^T(f_d) \omega_D^*(f_d) \left(\xi \tilde{\mathbf{a}} - \frac{\tilde{\mathbf{Z}} \omega_D^*(f_d)}{\omega_D^T(f_d) \omega_D^*(f_d)} \right)^\dagger \\ &\quad \times \left(\mathbf{I} + \tilde{\mathbf{Z}} \mathbf{P}_{\omega_D^*(f_d)}^\perp \tilde{\mathbf{Z}}^\dagger \right)^{-1} \tilde{\mathbf{a}}. \end{aligned} \quad (86)$$

Setting the result of (86) to zero, we can obtain the MLE of ξ under \mathcal{H}_1 , as

$$\hat{\xi} = \frac{\tilde{\mathbf{a}}^\dagger \left(\mathbf{I} + \tilde{\mathbf{Z}} \mathbf{P}_{\omega_D^*(f_d)}^\perp \tilde{\mathbf{Z}}^\dagger \right)^{-1} \tilde{\mathbf{Z}} \omega_D^*(f_d)}{\tilde{\mathbf{a}}^\dagger \left(\mathbf{I} + \tilde{\mathbf{Z}} \mathbf{P}_{\omega_D^*(f_d)}^\perp \tilde{\mathbf{Z}}^\dagger \right)^{-1} \tilde{\mathbf{a}} \omega_D^T(f_d) \omega_D^*(f_d)}. \quad (87)$$

Substituting (87) into (85), leads to

$$\begin{aligned}
h(\hat{\xi}) &= 1 - \frac{\left| \tilde{\mathbf{a}}^\dagger \left(\mathbf{I} + \tilde{\mathbf{Z}} \mathbf{P}_{\omega_{\mathbf{D}}^*(f_d)}^\perp \tilde{\mathbf{Z}}^\dagger \right)^{-1} \tilde{\mathbf{Z}} \omega_{\mathbf{D}}^*(f_d) \right|^2}{\tilde{\mathbf{a}}^\dagger \left(\mathbf{I} + \tilde{\mathbf{Z}} \mathbf{P}_{\omega_{\mathbf{D}}^*(f_d)}^\perp \tilde{\mathbf{Z}}^\dagger \right)^{-1} \tilde{\mathbf{a}} \omega_{\mathbf{D}}^T(f_d) \omega_{\mathbf{D}}^*(f_d)} \\
&\quad + \frac{\omega_{\mathbf{D}}^T(f_d) \tilde{\mathbf{Z}}^\dagger \left(\mathbf{I} + \tilde{\mathbf{Z}} \mathbf{P}_{\omega_{\mathbf{D}}^*(f_d)}^\perp \tilde{\mathbf{Z}}^\dagger \right)^{-1} \tilde{\mathbf{Z}} \omega_{\mathbf{D}}^*(f_d)}{\omega_{\mathbf{D}}^T(f_d) \omega_{\mathbf{D}}^*(f_d)} \\
&= 1 + \frac{\omega_{\mathbf{D}}^T(f_d) \tilde{\mathbf{Z}}^\dagger \left(\mathbf{I} + \tilde{\mathbf{Z}} \mathbf{P}_{\omega_{\mathbf{D}}^*(f_d)}^\perp \tilde{\mathbf{Z}}^\dagger \right)^{-1}}{\tilde{\mathbf{a}}^\dagger \left(\mathbf{I} + \tilde{\mathbf{Z}} \mathbf{P}_{\omega_{\mathbf{D}}^*(f_d)}^\perp \tilde{\mathbf{Z}}^\dagger \right)^{-1} \tilde{\mathbf{a}}} \\
&\quad \times \left[\tilde{\mathbf{a}}^\dagger \left(\mathbf{I} + \tilde{\mathbf{Z}} \mathbf{P}_{\omega_{\mathbf{D}}^*(f_d)}^\perp \tilde{\mathbf{Z}}^\dagger \right)^{-1} \tilde{\mathbf{a}} \mathbf{I} \right. \\
&\quad \left. - \tilde{\mathbf{a}} \tilde{\mathbf{a}}^\dagger \left(\mathbf{I} + \tilde{\mathbf{Z}} \mathbf{P}_{\omega_{\mathbf{D}}^*(f_d)}^\perp \tilde{\mathbf{Z}}^\dagger \right)^{-1} \right] \\
&\quad \times \frac{\tilde{\mathbf{Z}} \omega_{\mathbf{D}}^*(f_d)}{\omega_{\mathbf{D}}^T(f_d) \omega_{\mathbf{D}}^*(f_d)}. \tag{88}
\end{aligned}$$

Further, (84) can be written as (89), which is located on the first line of the next page.

Similarly, we can obtain the MLE of \mathbf{R} under the null hypothesis \mathcal{H}_0

$$\hat{\mathbf{R}}_0 = \frac{\mathbf{Z}\mathbf{Z}^\dagger + \mathbf{S}}{K(L+1)}. \tag{90}$$

Then, we have

$$\begin{aligned}
f(\mathbf{Z}, \mathbf{Y} \mid \hat{\mathbf{R}}_0, \mathcal{H}_0) &= \frac{\text{cont.}}{\det^{K(L+1)}(\mathbf{Z}\mathbf{Z}^\dagger + \mathbf{S})} \\
&= \frac{\text{cont.}}{\det^{K(L+1)}(\mathbf{S}) \det^{KL}(\tilde{\mathbf{Z}}\tilde{\mathbf{Z}}^\dagger + \mathbf{I})}. \tag{91}
\end{aligned}$$

Combining (83), (89) and (91) yields the OGLRT detector (14).

REFERENCES

- [1] P. Antonik, M. Wicks, H. Griffiths, and C. Baker, "Frequency diverse array radars," pp. 3 pp.–, 2006.
- [2] W. Wang, "Range-angle dependent transmit beampattern synthesis for linear frequency diverse arrays," *IEEE Transactions on Antennas and Propagation*, vol. 61, no. 8, pp. 4073–4081, 2013.
- [3] Y. Lang, Z. Yang, L. Yang, and X. Chen, "Lamb wave frequency diverse array," *IEEE Transactions on Ultrasonics, Ferroelectrics, and Frequency Control*, pp. 1–1, 2022.
- [4] R. Gui, B. Huang, W.-Q. Wang, and Y. Sun, "Generalized ambiguity function for FDA radar joint range, angle and doppler resolution evaluation," *IEEE Geoscience and Remote Sensing Letters*, vol. 19, pp. 1–5, 2022.
- [5] B. Huang, Y. Yan, A. Basit, W.-Q. Wang, and J. Cheng, "Radar cross section characterization of frequency diverse array radar," *IEEE Transactions on Aerospace and Electronic Systems*, pp. 1–11, 2022.
- [6] Y. Liao, H. Tang, X. Chen, and W. Q. Wang, "Frequency diverse array beampattern synthesis with taylor windowed frequency offsets," *IEEE Antennas and Wireless Propagation Letters*, vol. 19, no. 11, pp. 1901–1905, 2020.
- [7] Y. Liao, H. Tang, W.-q. Wang, and M. Xing, "A low sidelobe deceptive jamming suppression beamforming method with a frequency diverse array," *IEEE Transactions on Antennas and Propagation*, vol. 70, no. 6, pp. 4884–4889, 2022.
- [8] A. Basit, W. Wang, and S. Y. Nusenu, "Adaptive transmit beamspace design for cognitive FDA radar tracking," *IET Radar, Sonar Navigation*, vol. 13, no. 12, pp. 2083–2092, 2019.
- [9] L. Wang, W.-Q. Wang, H. Guan, and S. Zhang, "LPI property of FDA transmitted signal," *IEEE Transactions on Aerospace and Electronic Systems*, vol. 57, no. 6, pp. 3905–3915, 2021.
- [10] Y.-Q. Hu, H. Chen, S.-L. Ji, W.-Q. Wang, and H. Chen, "Adaptive detector for FDA-Based ambient backscatter communications," *IEEE Transactions on Wireless Communications*, vol. 21, no. 12, pp. 10 381–10 392, 2022.
- [11] S. Y. Nusenu, S. Huaizong, and P. Ye, "Power allocation and equivalent transmit FDA beamspace for 5G mmwave NOMA networks: Meta-heuristic optimization approach," *IEEE Transactions on Vehicular Technology*, vol. 71, no. 9, pp. 9635–9646, 2022.
- [12] B. Huang, A. Basit, R. Gui, and W.-Q. Wang, "Adaptive moving target detection without training data for FDA-MIMO radar," *IEEE Transactions on Vehicular Technology*, vol. 71, no. 1, pp. 220–232, 2021.
- [13] L. Lan, A. Marino, A. Aubry, A. De Maio, G. Liao, J. Xu, and Y. Zhang, "GLRT-based adaptive target detection in FDA-MIMO radar," *IEEE Transactions on Aerospace and Electronic Systems*, vol. 57, no. 1, pp. 597–613, 2020.
- [14] J. Xu, G. Liao, L. Huang, and H. C. So, "Robust adaptive beamforming for fast-moving target detection with FDA-STAP radar," vol. 65, no. 4, pp. 973–984, 2017.
- [15] E. Fishler, A. Haimovich, R. Blum, D. Chizhik, L. Cimini, and R. Valenzuela, "Mimo radar: An idea whose time has come," in *Proceedings of the 2004 IEEE Radar Conference (IEEE Cat. No. 04CH37509)*. IEEE, 2004, pp. 71–78.
- [16] J. Li and S. Petre, *MIMO Radar Signal Processing*. New York: John Wiley and Sons, 2009.
- [17] L. Lan, G. Liao, S. Zhu, and H.C.So, "Deceptive jamming suppression with frequency diverse MIMO radar," *Signal Processing*, vol. 113, no. aug., pp. 9–17, 2015.
- [18] J. Xiong, W. Wang, and K. Gao, "FDA-MIMO radar range-angle estimation: CRLB, MSE, and resolution analysis," *IEEE Transactions on Aerospace and Electronic Systems*, vol. 54, no. 1, pp. 284–294, 2018.
- [19] M. Tan, C. Wang, and Z. Li, "Correction analysis of frequency diverse array radar about time," *IEEE Transactions on Antennas and Propagation*, vol. 69, no. 2, pp. 834–847, 2021.
- [20] L. Lan, J. Xu, G. Liao, Y. Zhang, F. Fioranelli, and H. C. So, "Suppression of mainbeam deceptive jammer with FDA-MIMO radar," *IEEE Transactions on Vehicular Technology*, vol. 69, no. 10, pp. 11 584–11 598, 2020.
- [21] J. Xu, G. Liao, S. Zhu, L. Huang, and H. C. So, "Joint range and angle estimation using MIMO radar with frequency diverse array," *IEEE Transactions on Signal Processing*, vol. 63, no. 13, pp. 3396–3410, 2015.
- [22] J. Cheng, W.-Q. Wang, and S. Zhang, "Joint MIMO and frequency diverse array for suppressing mainlobe interferences," in *2020 International Symposium on Antennas and Propagation (ISAP)*. IEEE, 2021, pp. 171–172.
- [23] W. Wan, S. Zhang, and W.-Q. Wang, "Resolving doppler ambiguity of high-speed moving targets via FDA-MIMO radar," *IEEE Geoscience and Remote Sensing Letters*, vol. 19, pp. 1–5, 2022.
- [24] M. Zhang, G. Liao, J. Xu, X. He, Q. Liu, L. Lan, and S. Li, "High-resolution and wide-swath SAR imaging with sub-band frequency diverse array," *IEEE Transactions on Aerospace and Electronic Systems*, vol. 59, no. 1, pp. 172–183, 2022.
- [25] L. Huang, X. Li, W. Wan, S. Zhang, and W.-Q. Wang, "Frequency diverse array introduced into SAR GMTI to mitigate blind velocity and doppler ambiguity," *IEEE Geoscience and Remote Sensing Letters*, vol. 19, pp. 1–5, 2022.
- [26] B. Huang, W.-Q. Wang, S. Zhang, and Y. Liao, "FDA-Based space-time-frequency deceptive jamming against SAR imaging," *IEEE Transactions on Aerospace and Electronic Systems*, vol. 58, no. 3, pp. 2127–2140, 2021.
- [27] J. Jian, B. Huang, and W.-Q. Wang, "Physical-layer security with frequency diverse array for DF multi-antenna relaying SWIPT system," *International Journal of Electronics Letters*, vol. 0, no. 0, pp. 1–9, 2022.
- [28] S. Ji, W. Wang, H. Chen, and S. Zhang, "On physical-layer security of FDA communications over rayleigh fading channels," *IEEE Transactions on Cognitive Communications and Networking*, vol. 5, no. 3, pp. 476–490, 2019.
- [29] K. Wang, G. Liao, J. Xu, Y. Zhang, and L. Huang, "Clutter rank analysis in airborne FDA-MIMO radar with range ambiguity," *IEEE Transactions on Aerospace and Electronic Systems*, vol. 58, no. 2, pp. 1416–1430, 2021.

$$\begin{aligned}
\mathcal{G}(\hat{\xi}) &= \det \left[\mathbf{I} + \tilde{\mathbf{Z}}\tilde{\mathbf{Z}}^\dagger - \frac{\tilde{\mathbf{a}}\tilde{\mathbf{a}}^\dagger \left(\mathbf{I} + \tilde{\mathbf{Z}}\mathbf{P}_{\omega_D^*(f_d)}^\perp \tilde{\mathbf{Z}}^\dagger \right)^{-1} \tilde{\mathbf{Z}}\mathbf{P}_{\omega_D^*(f_d)} \tilde{\mathbf{Z}}^\dagger}{\tilde{\mathbf{a}}^\dagger \left(\mathbf{I} + \tilde{\mathbf{Z}}\mathbf{P}_{\omega_D^*(f_d)}^\perp \tilde{\mathbf{Z}}^\dagger \right)^{-1} \tilde{\mathbf{a}}} \right] \\
&= \det \left[\mathbf{I} + \tilde{\mathbf{Z}}\tilde{\mathbf{Z}}^\dagger \right] \det \left[\mathbf{I} - \frac{\left(\mathbf{I} + \tilde{\mathbf{Z}}\tilde{\mathbf{Z}}^\dagger \right)^{-1} \tilde{\mathbf{a}}\tilde{\mathbf{a}}^\dagger \left(\mathbf{I} + \tilde{\mathbf{Z}}\mathbf{P}_{\omega_D^*(f_d)}^\perp \tilde{\mathbf{Z}}^\dagger \right)^{-1} \tilde{\mathbf{Z}}\mathbf{P}_{\omega_D^*(f_d)} \tilde{\mathbf{Z}}^\dagger}{\tilde{\mathbf{a}}^\dagger \left(\mathbf{I} + \tilde{\mathbf{Z}}\mathbf{P}_{\omega_D^*(f_d)}^\perp \tilde{\mathbf{Z}}^\dagger \right)^{-1} \tilde{\mathbf{a}}} \right] \\
&= \det \left[\mathbf{I} + \tilde{\mathbf{Z}}\tilde{\mathbf{Z}}^\dagger \right] \left[1 - \frac{\tilde{\mathbf{a}}^\dagger \left(\mathbf{I} + \tilde{\mathbf{Z}}\mathbf{P}_{\omega_D^*(f_d)}^\perp \tilde{\mathbf{Z}}^\dagger \right)^{-1} \tilde{\mathbf{Z}}\mathbf{P}_{\omega_D^*(f_d)} \tilde{\mathbf{Z}}^\dagger \left(\mathbf{I} + \tilde{\mathbf{Z}}\tilde{\mathbf{Z}}^\dagger \right)^{-1} \tilde{\mathbf{a}}}{\tilde{\mathbf{a}}^\dagger \left(\mathbf{I} + \tilde{\mathbf{Z}}\mathbf{P}_{\omega_D^*(f_d)}^\perp \tilde{\mathbf{Z}}^\dagger \right)^{-1} \tilde{\mathbf{a}}} \right] \\
&= \det \left[\mathbf{I} + \tilde{\mathbf{Z}}\tilde{\mathbf{Z}}^\dagger \right] \frac{\tilde{\mathbf{a}}^\dagger \left(\mathbf{I} + \tilde{\mathbf{Z}}\tilde{\mathbf{Z}}^\dagger \right)^{-1} \tilde{\mathbf{a}}}{\tilde{\mathbf{a}}^\dagger \left(\mathbf{I} + \tilde{\mathbf{Z}}\mathbf{P}_{\omega_D^*(f_d)}^\perp \tilde{\mathbf{Z}}^\dagger \right)^{-1} \tilde{\mathbf{a}}}.
\end{aligned}$$

(89)

- [30] B. Huang, J. Jian, A. Basit, R. Gui, and W.-Q. Wang, "Adaptive distributed target detection for FDA-MIMO radar in gaussian clutter without training data," *IEEE Transactions on Aerospace and Electronic Systems*, vol. 58, no. 4, pp. 2961–2972, 2022.
- [31] R. Gui, W.-Q. Wang, A. Farina, and H. C. So, "Fda radar with doppler-spreading consideration: Mainlobe clutter suppression for blind-doppler target detection," *Signal Processing*, vol. 179, p. 107773, 2021.
- [32] B. Huang, A. Basit, W.-Q. Wang, and S. Zhang, "Adaptive detection with bayesian framework for fda-mimo radar," *IEEE Geoscience and Remote Sensing Letters*, vol. 19, pp. 1–5, 2022.
- [33] J. Xu, S. Zhu, and G. Liao, "Space-time-range adaptive processing for airborne radar systems," *IEEE Sensors Journal*, vol. 15, no. 3, pp. 1602–1610, 2014.
- [34] —, "Range ambiguous clutter suppression for airborne FDA-STAP radar," *IEEE Journal of Selected Topics in Signal Processing*, vol. 9, no. 8, pp. 1620–1631, 2015.
- [35] J. Xu, G. Liao, and H. C. So, "Space-time adaptive processing with vertical frequency diverse array for range-ambiguous clutter suppression," *IEEE Transactions on Geoscience and Remote Sensing*, vol. 54, no. 9, pp. 5352–5364, 2016.
- [36] J. Zhu, S. Zhu, J. Xu, L. Lan, K. Yu, and Y. Xu, "Target detection in mainlobe jammers with fda-mimo radar," in *2023 IEEE International Radar Conference (RADAR)*, 2023, pp. 1–6.
- [37] L. Zeng, Y.-L. Wang, W. Liu, J. Liu, and L. Lan, "GLRT-based detectors for fda-mimo radar with training data," *Digit. Signal Process.*, vol. 130, p. 103729, 2022. [Online]. Available: <https://api.semanticscholar.org/CorpusID:252230962>
- [38] W. Liu, W. Xie, and Y. Wang, "Parametric detector in the situation of mismatched signals," *IET Radar, Sonar and Navigation*, vol. 8, pp. 48–53, 2014.
- [39] A. De Maio, "Rao test for adaptive detection in Gaussian interference with unknown covariance matrix," *IEEE transactions on signal processing*, vol. 55, no. 7, pp. 3577–3584, 2007.
- [40] —, "A new derivation of the adaptive matched filter," *IEEE Signal Processing Letters*, vol. 11, no. 10, pp. 792–793, 2004.
- [41] F. C. Robey, D. R. Fuhrmann, E. J. Kelly, and R. Nitzberg, "A CFAR adaptive matched filter detector," *IEEE Transactions on aerospace and electronic systems*, vol. 28, no. 1, pp. 208–216, 1992.
- [42] J. Liu and J. Li, "Robust detection in mimo radar with steering vector mismatches," *IEEE Transactions on Signal Processing*, vol. 67, no. 20, pp. 5270–5280, 2019.
- [43] W. Liu, W. Xie, J. Liu, and Y. Wang, "Adaptive double subspace signal detection in gaussian background—part i: Homogeneous environments," *IEEE Transactions on Signal Processing*, vol. 62, no. 9, pp. 2345–2357, 2014.
- [44] E. J. Kelly and K. W. Forsythe, "Adaptive detection and parameter estimation for multidimensional signal models," 1989.
- [45] R. Gui, W.-Q. Wang, C. Cui, and H. C. So, "Coherent pulsed-FDA radar receiver design with time-variance consideration: SINR and CRB analysis," *IEEE Transactions on Signal Processing*, vol. 66, no. 1, pp. 200–214, 2017.
- [46] R. Gui, W.-Q. Wang, and Z. Zheng, "Low-complexity GLRT for FDA radar without training data," *Digital Signal Processing*, vol. 107, p. 102861, 2020. [Online]. Available: <https://www.sciencedirect.com/science/article/pii/S1051200420302062>
- [47] E. J. Kelly, "An adaptive detection algorithm," *IEEE transactions on aerospace and electronic systems*, no. 2, pp. 115–127, 1986.
- [48] S. M. Kay, *Fundamentals of statistical signal processing: estimation theory*. Prentice-Hall, Inc., 1993.
- [49] X.-D. Zhang, *Matrix analysis and applications*. Cambridge University Press, 2017.
- [50] A. De Maio, M. S. Greco, and Eds, *Modern Radar Detection Theory*. Radar, Sonar and Navigation. Stevenage, U.K.: Inst. Eng. Technol, 2015.
- [51] F. Bandiera, D. Orlando, and G. Ricci, *Advanced radar detection schemes under mismatched signal models*. Springer Nature, 2022.
- [52] T. Anderson, "An introduction to multivariate statistical analysis, 2 wiley, new york," *TW Anderson*, vol. 25, pp. 643–665, 1984.
- [53] E. J. Kelly, "Finite-sum expressions for signal detection probabilities," 1981. [Online]. Available: <https://api.semanticscholar.org/CorpusID:119057852>
- [54] Y. Gu and A. Leshem, "Robust adaptive beamforming based on interference covariance matrix reconstruction and steering vector estimation," *IEEE Transactions on Signal Processing*, vol. 60, no. 7, pp. 3881–3885, 2012.
- [55] S. Sun, J. Liu, W. Liu, and T. Jian, "Robust detection of distributed targets based on rao test and wald test," *Signal Processing*, vol. 180, p. 107801, 2021.
- [56] S. Bose and A. O. Steinhardt, "Adaptive array detection of uncertain rank one waveforms," *IEEE Transactions on Signal Processing*, vol. 44, no. 11, pp. 2801–2809, 1996.
- [57] W. Liu, W. Xie, J. Liu, and Y. Wang, "Adaptive double subspace signal detection in gaussian background—part ii: Partially homogeneous environments," *IEEE Transactions on Signal Processing*, vol. 62, no. 9, pp. 2358–2369, 2014.